


LncRNA SNHG1 knockdown inhibits hyperglycemia induced ferroptosis *via* miR-16-5p/ACSL4 axis to alleviate diabetic nephropathy

Xiangdong Fang¹, Jianling Song¹, Yanxia Chen¹, Shuying Zhu¹, Weiping Tu¹, Ben Ke^{1*} , Lidong Wu^{2*}

¹Department of Nephrology, The Second Affiliated Hospital of Nanchang University, Nanchang, Jiangxi Province, China, and ²Emergency Department, The Second Affiliated Hospital of Nanchang University, Nanchang, Jiangxi Province, China

Keywords

Diabetic nephropathy, LncRNA SNHG1, miR-16-5p

*Correspondence

Ben Ke
Tel: +86-15270882765
E-mail address:
keben-1989125@163.com
Lidong Wu
Tel: +86-13807095219
E-mail address:
dongguawu89@163.com

J Diabetes Investig 2023; 14: 1056–1069

doi: [10.1111/jdi.14036](https://doi.org/10.1111/jdi.14036)

ABSTRACT

Background: Hyperglycemia accelerates the development of diabetic nephropathy (DN) by inducing renal tubular injury. Nevertheless, the mechanism has not been elaborated fully. Here, the pathogenesis of DN was investigated to seek novel treatment strategies.

Methods: A model of diabetic nephropathy was established *in vivo*, the levels of blood glucose, urine albumin creatinine ratio (ACR), creatinine, blood urea nitrogen (BUN), malondialdehyde (MDA), glutathione (GSH), and iron were measured. The expression levels were detected by qRT-PCR and Western blotting. H&E, Masson, and PAS staining were used to assess kidney tissue injury. The mitochondria morphology was observed by transmission electron microscopy (TEM). The molecular interaction was analyzed using a dual luciferase reporter assay.

Results: SNHG1 and ACSL4 were increased in kidney tissues of DN mice, but miR-16-5p was decreased. Ferrostatin-1 treatment or SNHG1 knockdown inhibited ferroptosis in high glucose (HG)-treated HK-2 cells and in db/db mice. Subsequently, miR-16-5p was confirmed to be a target for SNHG1, and directly targeted to ACSL4. Overexpression of ACSL4 greatly reversed the protective roles of SNHG1 knockdown in HG-induced ferroptosis of HK-2 cells.

Conclusions: SNHG1 knockdown inhibited ferroptosis *via* the miR-16-5p/ACSL4 axis to alleviate diabetic nephropathy, which provided some new insights for the novel treatment of diabetic nephropathy.

INTRODUCTION

Diabetic nephropathy (DN) is one of the most common complications of diabetes, which is a key cause of kidney failure^{1,2}. Diabetic nephropathy has a high incidence, and it is reported that about one quarter of patients with diabetes will eventually develop diabetic nephropathy³. Long-term hyperglycemia is the main cause of diabetic nephropathy⁴. It is a pity that diabetic nephropathy lacks targeted treatment strategies⁵. Therefore, understanding the pathogenesis of diabetic nephropathy is helpful to seek new therapeutic strategies.

Long non-coding RNA (lncRNA) is closely associated with the progression of diabetic nephropathy⁶. LncRNA GAS5 overexpression inhibited mesangial cell proliferation and fibrosis⁷. LncRNA NR_038323 repressed the renal fibrosis of diabetic nephropathy by sponging miR-324-3p⁸. Small nucleolar RNA host gene 1 (SNHG1) is a novel lncRNA located at chromosome 11q12.3 and functions in attenuating inflammation during ischemic stroke⁹. Moreover, SNHG1 could regulate IL-1 β -induced arthritis¹⁰. Notably, a previous study demonstrated that SNHG1 regulated various ferroptosis-related genes in liver cancer¹¹. Nevertheless, the function of SNHG1 in diabetic nephropathy is still unknown.

Received 1 February 2023; revised 26 April 2023; accepted 18 May 2023

MicroRNAs (miRNAs) regulate gene expression after transcription by binding to 3'-UTR of the target gene¹². MiRNA is reported to be involved in the progression of renal fibrosis^{13,14}. A previous study showed that miR-21 inhibited renal fibrosis in diabetic nephropathy progression by negatively targeting BMP-7¹⁵. miR-16-5p was down-regulated in patients with diabetic nephropathy¹⁶, and its overexpression attenuated the development of diabetic nephropathy by reducing podocyte apoptosis¹⁷. Importantly, bioinformatics analysis also showed the physical interaction between SNHG1 and miR-16-5p. In addition, it was reported previously that miR-16-5p regulated ferroptosis by targeting SLC7A11 in adriamycin-induced ferroptosis in cardiomyocytes¹⁸. However, whether SNHG1 regulates diabetic nephropathy *via* sponging miR-16-5p remains unclear.

Ferroptosis, a new type of programmed cell death characterized by lipid peroxides and reactive oxygen species (ROS) accumulation^{19,20}, is involved in the occurrence and development of various diseases^{20,21}. Increasing evidence indicates that high glucose (HG) caused oxidative stress by increasing the production of ROS, thus inducing ferroptosis and accelerating the development of diabetic nephropathy^{22,23}. However, its underlying mechanism remains unclear. Acyl-CoA synthetase long chain family member 4 (ACSL4), an important regulator of ferroptosis, is highly expressed in DN mice, and overexpressed-ACSL4 led to ferroptosis²⁴. ACSL4 has been identified as a biomarker and contributor of ferroptosis²⁵. In diabetic nephropathy, the down-regulation of ACSL4 means that ferroptosis was inhibited, indicating that the progression of diabetic nephropathy was alleviated²⁶. Although the function of ACSL4-mediated ferroptosis in diabetic nephropathy has been well defined, the underlying regulatory mechanism remains a question of interest.

In summary, previous bioinformatics findings revealed a physical interaction between SNHG1 and miR-16-5p, or miR-16-5p and ACSL4. Thus, we hypothesized that SNHG1 might regulate the progression of diabetic nephropathy *via* the miR-16-5p/ACSL4 axis. We studied the regulatory effect of SNHG1 on ferroptosis, which might provide a new direction for the treatment of diabetic nephropathy.

MATERIALS AND METHODS

Establishment of a mouse model with diabetes

CasGene Biotech company (Beijing, China) provided 8-week-old male C57BLKs/J db/m and db/db mice. All animal experiments and protocols were reviewed and approved by the Animal Care and Use Committee of the Second Affiliated Hospital of Nanchang University. After acclimation for 1 week, the mice were randomly divided into five groups ($n = 8$): (1) db/m group: db/m mice were untreated; (2) db/db group: db/db mice were untreated; (3) db/db + ferrostatin-1 group: db/db mice were injected with ferrostatin-1, a ferroptosis inhibitor, intraperitoneally (1 mg/kg, weekly) for 12 weeks starting at 12 weeks of age; (4) db/db + shNC group: db/db mice were tail vein

injected with 100 μ L lentivirus-packaged shNC vectors every week (Sangon Biotech, Shanghai, China, 1×10^8 TU/mL) for 12 weeks starting at 12 weeks of age; (5) db/db + shSNHG1 group: db/db mice were tail vein injected with 100 μ L lentivirus-packaged shSNHG1 vectors every week (Sangon Biotech, 1×10^8 TU/mL) for 12 weeks starting at 12 weeks of age. After intervention, the blood samples of these mice were obtained every 4 weeks. 12 weeks later, when the mice reached 24 weeks of age, urine and blood samples were collected, and the mice were killed by intraperitoneal injection of 30 mg/kg sodium pentobarbital (Sigma-Aldrich, St Louis, MO, USA) after weighing to collect kidney tissues. Serum was separated by centrifugation at $3000 \times g$ for 15 min and subjected to a glucose analyzer to measure blood glucose (Roche, Germany). Moreover, mouse BUN assay kit (Solarbio, Beijing, China) and a mouse Cr ELISA kit (Senbeijia Biological Technology Co., Ltd, Nanjing, China) were used to detect BUN, urinary creatinine, and serum creatinine levels, respectively, according to the protocol instructions.

H&E staining

The kidney tissue was fixed with 4% paraformaldehyde overnight and cut into 5 μ m thick sections. Then the sections were dehydrated with gradient alcohol, washed, and embedded in paraffin. The sections were subsequently stained with hematoxylin for 10 min and eosin for 5 min. Sections were observed and photographed under a microscope (BD Pharmingen, San Diego, California). The glomerular size was detected to illustrate the degree of glomerular hypertrophy. The degree of damage of the tubules was evaluated by a widened lumen, atrophy, and thickened basement membranes.

Masson staining

The paraffin sections of the kidney tissues (4 μ m) were prepared and incubated overnight with Boyne solution. The sections were subsequently stained with Weigert iron hematoxylin solution and then stained with scarlet acid fuchsin solution. The slices were differentiated with acetic acid solution, soaked in 2% green light solution and patched with Eukitt. Finally, an Aperio ScanScope CS2 device was used to acquire digital slides. Masson staining evaluated the degree of renal fibrosis by measuring the relative number of pixels (blue).

PAS staining

The samples were incubated with 0.1% periodic acid for 10 min, washed and incubated with Schiff's reagent for 17 min. After being washed, the samples were counterstained with Mayer's hematoxylin for 2 min and dehydrated. Finally, the samples were cleared in xylene and mounted with Entellan. PAS staining illustrated the mesangial matrix expansion. Mesangial matrix expansion was semi-quantitatively evaluated by measuring the relative number of pixels (pink area) divided by the total area of the glomerulus.

***In situ* hybridization (ISH) and fluorescence *in situ* hybridization (FISH) assays**

The SNHG1 expression was measured in paraffin-embedded kidney samples using an ISH optimization kit (Roche, Basel, Switzerland) according to the manufacturer's instructions. The locked nucleic acid (LNA)-modified oligonucleotide probe targeting SNHG1 was designed and synthesized at Exiqon (Vedbaek, Denmark). Briefly, kidney samples were treated with pepsin for 10 min at room temperature and incubated with 500 nM of probe at 55°C for 4 h. The samples were incubated with blocking solution for 30 min, anti-digoxigenin (anti-DIG) reagent was applied for 60 min. After being washed, the sections were incubated with 3,3'-diaminobenzidine (DAB), and counterstaining was performed using hematoxylin. Quantification was performed by examining the percentage of positive cells.

The images were acquired with a fluorescence microscope (IX70, Olympus, Japan). The subcellular localization of SNHG1 in HK-2 cells was analyzed by the FISH assay. In brief, HK-2 cells were fixed and incubated with 20 μ L hybridizing solution at 42°C overnight. Then, the blocking solution was dripped at 37°C for 30 min. Biotinylated anti-digoxin was also dripped at 37°C for another 60 min. The nuclei were stained with DAB. The subcellular localization of SNHG1 was observed under an Olympus IX-71 microscope (Tokyo, Japan).

Cell culture, treatment, and transfection

Human renal tubular epithelial cells (HK-2), mouse mesangial cells (SV40-MES13), and mouse podocytes (MPC5), obtained from Chinese Academy of Sciences Cell Bank (Shanghai, China), were cultured in DMEM/F12 (Invitrogen, CA, Carlsbad, CA, USA) containing 10% FBS (Invitrogen) at 37°C with 5% CO₂. The SV40-MES13 and MPC5 cells were cultured in DMEM (Invitrogen) containing 10% FBS (Invitrogen) at 37°C with 5% CO₂. Subsequently, the cells were incubated with normal glucose (Sigma-Aldrich, NG; 5.5 mM), a high concentration of mannose (Sigma-Aldrich, OS; 5.5 mM glucose and 19.5 mM mannose), and a high glucose (HG; 25 mM) for 48 h, respectively. The shRNA against SNHG1, overexpressing vectors of ACSL4 (pcDNA3.1-ACSL4, OE-ACSL4), miR-16-5p mimics or inhibitor as well as the negative controls, purchased from GenePharma (Shanghai, China) were transfected into cells using Lipofectamine 3000 (Invitrogen) for 48 h.

Transmission electron microscopy (TEM)

The HK-2 cells were fixed with 2% glutaraldehyde for 12 h, washed with PBS and then fixed with 1% samarium tetroxide for 2 h. The cells were subsequently dehydrated with ethanol and stained with toluidine blue. The morphology of mitochondria was observed under TEM.

Iron, GSH, and MDA assay

10 mg kidney tissue was taken from each group and rinsed with saline. The tissue was homogenized and immediately mixed with cold salt water. Then the cells were collected,

homogenized with an ultrasonic cell pulverizer, and centrifuged for 10 min to collect the supernatant. Similarly, the cells were collected and homogenized with ultrasonic cell pulverizer, and centrifuged for 10 min to collect the supernatant. Subsequently, an iron assay kit, a micro malondialdehyde assay kit (Solarbio, Beijing, China), and a GSH assay kit (Beyotime, Nanjing, China) were used to assess the iron level, MDA activity, and GSH levels, respectively, according to a previous study¹⁹.

RIP assay

The RIP assay was performed using the Magna RIP RNA binding protein immunoprecipitation kit (Millipore, Bedford, MA, USA). The HK-2 cells were lysed, and the cell lysates were incubated with magnetic beads coupled with AGO2 antibody or negative control IgG antibody (Millipore). Then, the RNA of immunoprecipitation was extracted and subjected to qRT-PCR analysis.

Dual-luciferase gene reporter assay

SNHG1 and ACSL4 3'-UTR fragments containing miR-16-5p wild-type (Wt) binding site or miR-16-5p mutation binding site (Mut) were amplified by PCR, and inserted into pmirGLO vector (Promega, Fitchburg, WI, USA) to construct ACSL4-Wt, ACSL4-Mut, SNHG1-Wt, and SNHG1-Mut. Then, the HK-2 cells were co-transfected with constructed luciferase reporter vectors and miR-16-5p mimics/mimics NC. The luciferase activity was subsequently examined by a double luciferase reporter kit (Promega) and normalized to renilla luciferase activity.

Immunohistochemistry

The kidney tissue sections (4 μ m in thickness) were prepared. After deparaffinization and antigen retrieval (Dako, CA, USA), the sections were then blocked and incubated with antibody against ACSL4 (Abcam, Cambridge, UK, 1:500) for 1 h followed by incubation with an appropriate secondary antibody (Abcam, 1:1000) for 1 h. The sections were stained with DAB and then counterstained, dehydrated, and mounted. The images were taken using a microscope. Images quantified by Image-Pro Plus 6.0 analysis software.

Subcellular fractionation analysis

A PARIS™ kit (Invitrogen, Waltham, USA) was used for subcellular fractionation analysis. Cytoplasmic and nuclear grades were isolated from HK-2 cells with nuclear and cytoplasmic extraction reagents (Beyotime, Nanjing, China). qRT-PCR was carried out to analyze cytoplasmic and nuclear RNA extracts, and GAPDH and U6 were used as the reference genes.

qRT-PCR

After the total RNA was extracted with TRIZOL reagent (Takara, Osaka, Japan), miRNAs were collected by the miRNA isolation kit (Takara, Osaka, Japan), and detected using a Taqman miRNA assay kit (Takara). The cDNA was synthesized using the M-MLV reverse transcriptase (Invitrogen, CA, USA) and subjected to qRT-PCR assay with SYBR (Takara). The expressions of U6 and

GAPDH are stable under various extreme conditions²⁷. Therefore, GAPDH and U6 were used as the reference gene for mRNAs and miRNAs in our study. The data were analyzed with the $2^{-\Delta\Delta CT}$ method. The primers used in the study are shown in Table 1.

Western blot

The total proteins were extracted using RIPA lysis buffer and quantified by a BCA kit (Beyotime, Nanjing, China). Subsequently, the total protein (30 μ g) was isolated by 10% SDS-PAGE and transferred to a PVDF membrane (Invitrogen, CA, USA). Then, the membranes were incubated overnight with rabbit anti-ACSL4, anti-SLC7A11, anti-GPX4, anti-collagen I, anti-collagen IV and anti-fibronectin. After being washed with PBS-T, the membranes were then incubated with secondary antibody for 60 min. The immunoblots were visualized by GEL imaging system and quantified by Image J software v1.49. All antibodies were purchased from Abcam (Cambridge, UK, 1:1000).

Statistical analysis

Mean \pm SD represents data from at least three independent trials. Student's *t*-test or one-way analysis of variance (ANOVA) with Turkey *post hoc* test were used to compare differences between two or multiple groups, respectively. A value of $P < 0.05$ was considered statistically significant.

RESULTS

SNHG1 and ACSL4 were highly expressed in DN mice

Firstly, the DN mouse was established to show that blood glucose was significantly increased in db/db mice (Figure 1a). The urine ACR level and serum creatinine and BUN levels were also enhanced in db/db mice (Figure 1b–d). Subsequently, pathological staining and immunohistochemical staining analysis indicated that the mesangial cells had proliferated, the mesangial extracellular matrix was increased, the basement membrane was thickened, and fibrous tissue had proliferated and infiltrated, as well as there being collagen deposition in the kidney tissues of db/db mice (Figure 1e). Neutrophil gelatinase-associated lipocalin (NGAL) and kidney injury molecule-1 (KIM-1) are markers of renal tubular injury²⁸. Herein, it was observed that NGAL and KIM-1 were increased significantly in kidney tissues of db/db mice (Figure 1f), indicating that the DN mouse model had been successfully established. Furthermore, the MDA and iron levels were higher in the kidney tissues of DN mice, but the GSH level was lower (Figure 1g). The protein level of ACSL4 was increased in the kidney tissues of DN mice (Figure 1h), indicating that diabetic nephropathy might be related to ferroptosis. Additionally, SNHG1 was increased in DN mice (Figure 1i). It also turned out that SNHG1 was expressed in both the nuclear and cytoplasm in kidney tissues, but mainly in the cytoplasm (Figure 1j).

Table 1 | Primers used for qRT-PCR analysis

Genes	Primer sequences (5'-3')
m-SNHG1-F	TCCTGGTGACAAATCTCAGGC
m-SNHG1-R	TGGTACGGCTCCTTTGTCTC
h-SNHG1-F	TGCAATGTTGAGCCCAACAAG
h-SNHG1-R	TGAGCCAAGCAGGTTATTGGT
hsa-miR-199a-3p-F	GCCGAGACAGTAGTCTGCACAT
hsa-miR-199a-3p-R	GTCGTATCCAGTGCAGGGTCCGAGGTATTCGACTGGATACGAC TAACCA
hsa-miR-424-5p-F	GCCGAGCAGCAGCAATTCATGT
hsa-miR-424-5p-R	GTCGTATCCAGTGCAGGGTCCGAGGTATTCGACTGGATACGAC TTCAA
hsa-miR-16-5p-F	GCCGAGTAGCAGCACGTAATA
hsa-miR-16-5p-R	GTCGTATCCAGTGCAGGGTCCGAGGTATTCGACTGGATACGACCCGCCAA
mmu-miR-16-5p-F	GCCGAGTAGCAGCACGTAATA
mmu-miR-16-5p-R	GTCGTATCCAGTGCAGGGTCCGAGGTATTCGACTGGATACGACCCGCCAA
h-ACSL4-F	CCGACCTAAGGGAGTGATGA
h-ACSL4-R	CCTGCAGCCATAGGTAAGC
m-ACSL4-F	AAGAAAGGCTATGACGCCCC
m-ACSL4-R	TCAGCCCATATCCCTGACCA
m-NGAL-F	GAAGTGTATCCCTGCCCCAT
m-NGAL-R	TTCTGATCCAGTAGCGACAGC
m-KIM-1-F	TGCCATCTTCTGCTTGCA
m-KIM-1-R	GGACGTGTGGGAATCTCTGG
U6-F	CTCGCTTCGGCAGCAC
U6-R	AACGCTTCACGAATTTGCGT
m-GAPDH-F	AGCCCAAGATGCCCTTCAGT
m-GAPDH-R	CCGTGTTCTACCCCAATG
h-GAPDH-F	CCAGGTGGTCTCTCTGA
h-GAPDH-R	GCTGTAGCCAAATCGTTGT

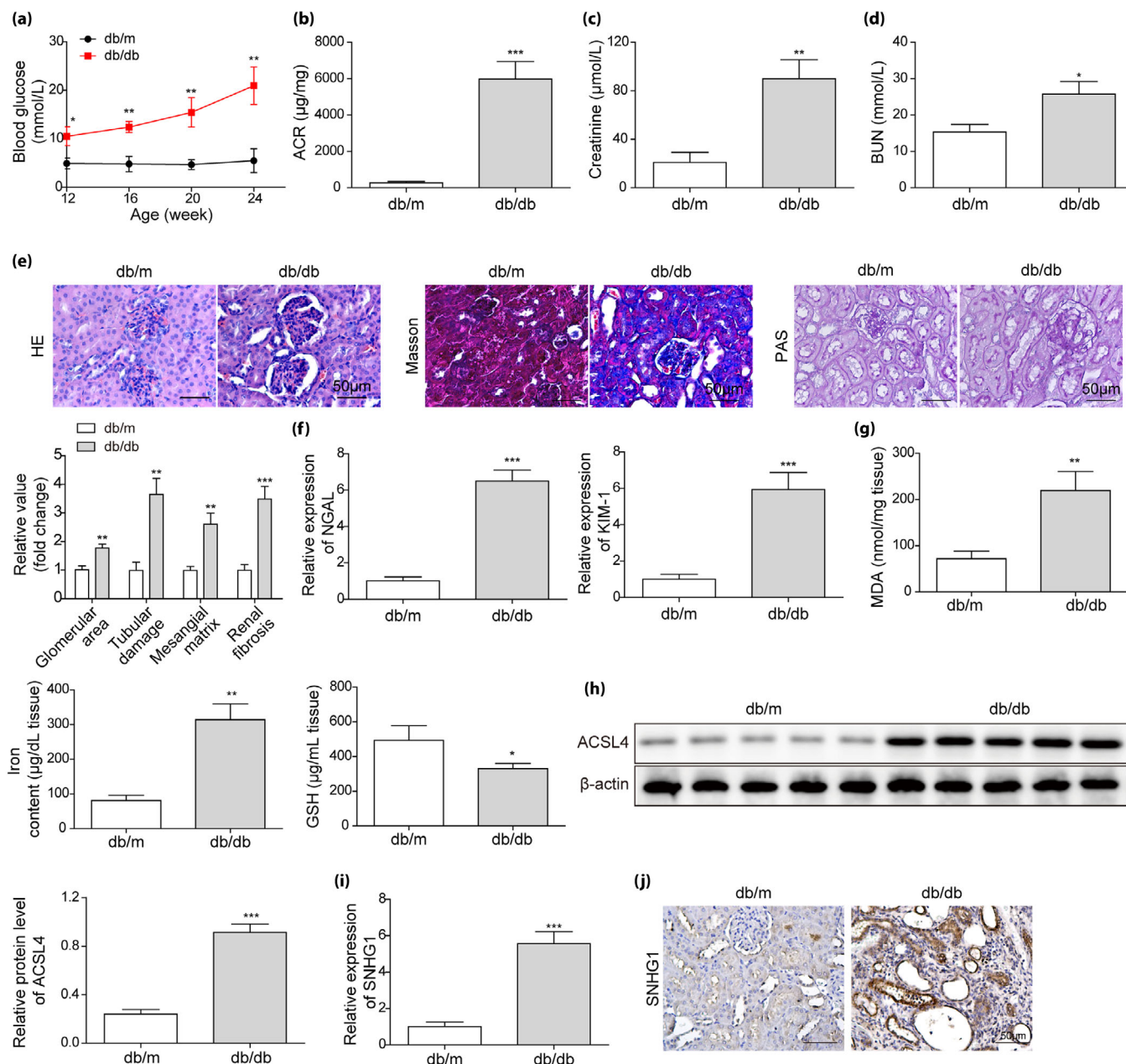


Figure 1 | SNHG1 and ACSL4 were highly expressed in DN mice. Mice model with diabetes (DN mice) was established. (a) Detection of blood glucose. (b) Ratio of urinary albumin to creatinine (ACR). (c,d) ELISA was performed to detect creatinine and BUN levels. (e) H&E, PAS, and Masson staining was used to assess renal tissue injury. (f) NGAL and KIM-1 levels were detected by qRT-PCR. (g) Detection of iron, GSH, and MDA. (h) Western blotting was performed to measure ACSL4 level. (i) SNHG1 expression was assessed by qRT-PCR. (j) SNHG1 localization in kidney tissue was detected using ISH assay. * $P < 0.05$, ** $P < 0.01$, and *** $P < 0.001$.

HG induced ferroptosis in HK-2 cells

The MDA and iron levels in the HG group were higher than that in the NG group, but GSH had the reverse trend (Figure 2a). The ACSL4, collagen I, collagen IV, and fibronectin levels were significantly up-regulated in the HG group, and the SLC7A11 and GPX4 levels were decreased (Figure 2b). Furthermore, the SNHG1 level in the HG group was higher than that in the NG group (Figure 2c), and SNHG1 was mainly located

in the cytoplasm in HK-2 cells (Figure 2d,e). These findings showed that HG triggered ferroptosis in HK-2 cells, and might be correlated with SNHG1 up-regulation.

SNHG1 knockdown inhibited HG-induced cell ferroptosis

Firstly, SNHG1 was knocked down in HK-2, SV40-MES13, and MPC5 cells by transfecting shSNHG1 (Figure 3a and Figure S1a). The levels of MDA and iron were increased

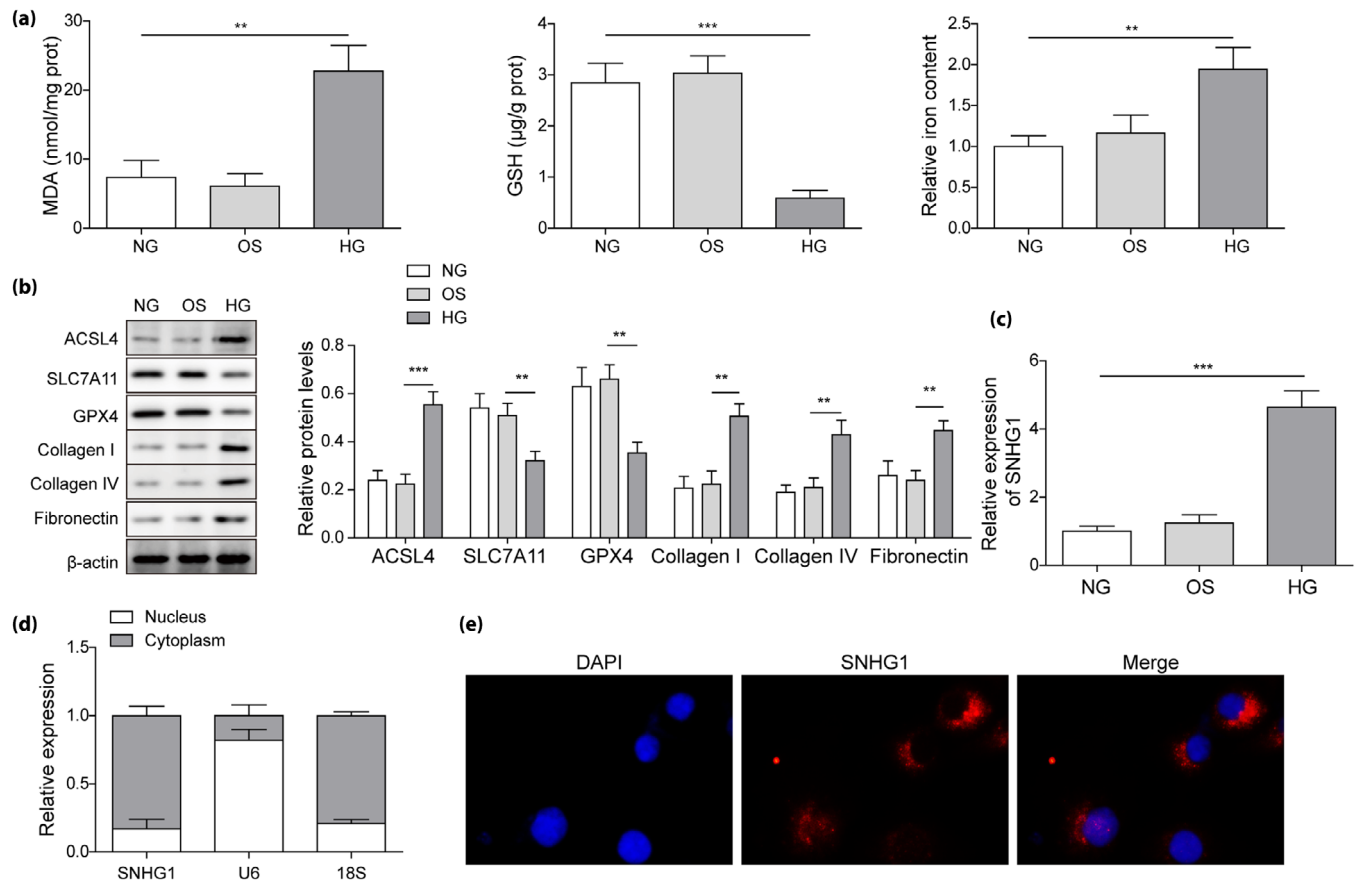


Figure 2 | High glucose (HG) induced ferroptosis of HK-2 cells. HK-2 cells were incubated with normal glucose, high mannose or HG for 48 h. (a) Detection of iron, GSH, and MDA. (b) ACSL4, SLC7A11, GPX4, collagen I, collagen IV, and fibronectin levels were measured by Western blotting. (c) SNHG1 expression was tested by qRT-PCR (d) The subcellular localization of SNHG1 was analyzed by subcellular fractionation analysis. (e) SNHG1 localization in cells was assessed FISH. $**P < 0.01$ and $***P < 0.001$.

significantly, but GSH expression was significantly decreased in HG or erastin-induced HK-2 cells, mouse mesangial cells, and mouse podocytes. SNHG1 knockdown or ferrostatin-1 (a ferroptosis inhibitor) reversed the effect of HG or erastin induction on the levels of MDA, iron, and GSH in HK-2, SV40-MES13, and MPC5 cells (Figure 3b and Figure S1b). Moreover, ACSL4, collagen I, collagen IV, and fibronectin levels were significantly up-regulated and SLC7A11 and GPX4 were decreased in HG or erastin-induced HK-2, SV40-MES13, and MPC5 cells, but these trends were antagonized by SNHG1 knockdown or ferrostatin-1 treatment (Figure 3c and Figure S1c). These findings suggested that SNHG1 knockdown inhibited HG-induced ferroptosis of HK-2 cells.

SNHG1 targeted to miR-16-5p and ACSL4 served as a target for miR-16-5p

Research has shown that miR-16-5p could inhibit HG-induced apoptosis in podocytes, and played a protective role in DN progression¹⁷. As shown in Figure 4a, the target miRNA downstream of SNHG1 was analyzed by starBase and RNAinter

databases, and the target miRNA upstream of ACSL4 was analyzed by starBase and Targetscan databases. Then, it was found that there were seven miRNAs (miR-199a-3p, miR-3,127-5p, miR-195-5p, miR-16-5p, miR-424-5p, miR-15b-5p, and miR-145-5p) in the intersection. In order to satisfy the mechanism of lncRNA regulating the expression of miRNA downstream target genes by combining miRNA, we selected miRNA with reduced expression in diabetic nephropathy (miR-199a-3p, miR-16-5p, miR-424-5p) by reviewing the literature. Then, we detected the expression levels of the above three miRNAs after SNHG1 knockdown, and the results showed that the increase of miR-16-5p was the most significant after SNHG1 knockdown (Figure 4b). Therefore, miR-16-5p was selected as the potential target of SNHG1 in regulating the progression of diabetic nephropathy. Bioinformatics analysis showed that there was an interaction between SNHG1 and miR-16-5p (Figure 4c). The qRT-PCR data showed that miR-16-5p was inhibited by HG induction (Figure 4d). The RIP assay proved the physical interaction between SNHG1 and miR-16-5p in HK-2 cells (Figure 4e). As shown in Figure 4f, miR-16-5p

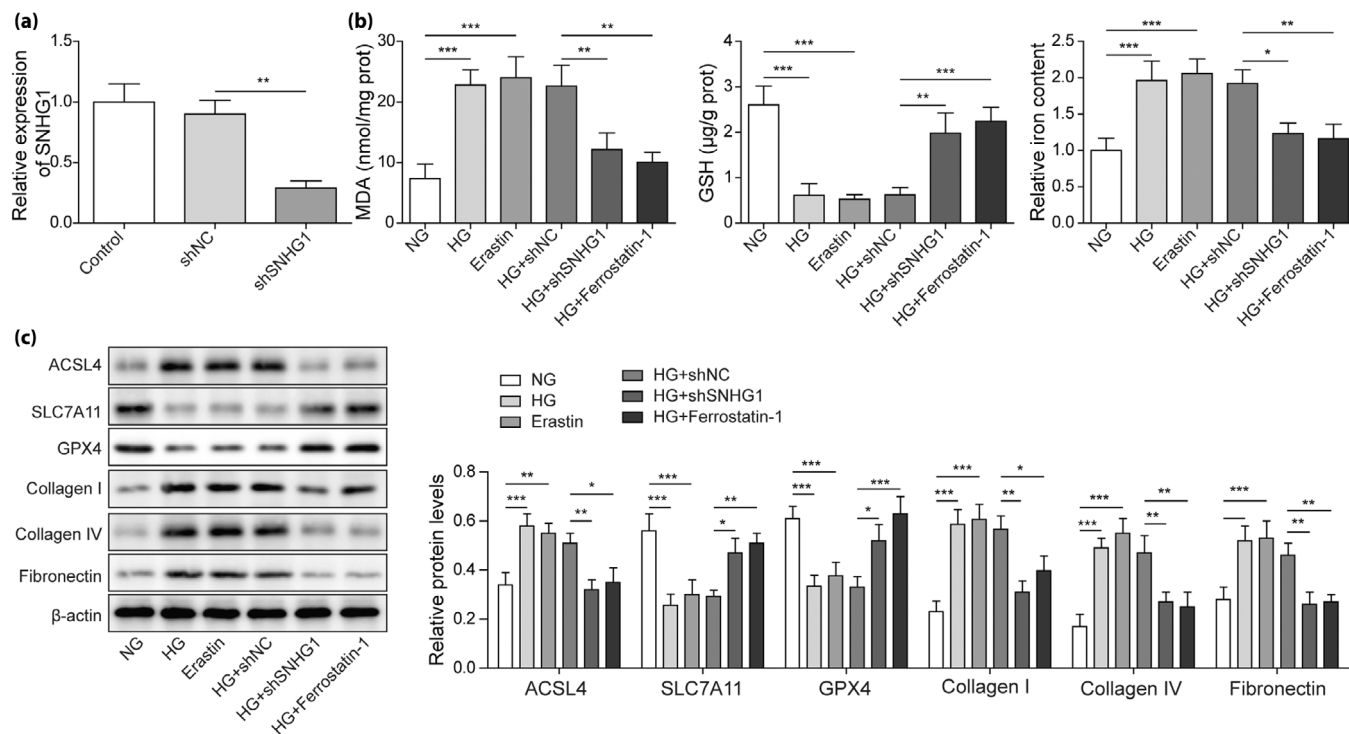


Figure 3 | SNHG1 knockdown inhibited HG-induced ferroptosis of HK-2 cells. HK-2 cells were transfected with shSNHG1 or shNC. (a) qRT-PCR was performed to assess SNHG1 level. HK-2 cells were divided into six groups: NG group, HG group, erastin group (positive control), HG + shNC group, HG + shSNHG1 group, and HG + ferrostatin-1 group. (b) Detection of iron, GSH, and MDA. (c) ACSL4, SLC7A11, GPX4, collagen I, collagen IV, and fibronectin levels were measured by Western blotting. * $P < 0.05$, ** $P < 0.01$ and *** $P < 0.001$.

overexpression reduced the luciferase activity in the SNHG1-WT group but had no significant effect on that of the SNHG1-MUT group (Figure 4f). Additionally, the starBase database predicted the binding sites between miR-16-5p and ACSL4 (Figure 4g). miR-16-5p mimics the remarkably increased miR-16-5p and down-regulated ACSL4 expression, while miR-16-5p knockdown greatly decreased miR-16-5p and up-regulated ACSL4 expression (Figure 4h-j). The dual luciferase reporter assay indicated that miR-16-5p directly bound with ACSL4 (Figure 4k). Collectively, the present evidence demonstrated that SNHG1 played as a sponge of miR-16-5p to competitively promote ACSL4 expression.

SNHG1 knockdown inhibited HG-induced ferroptosis of HK-2 cells via ACSL4

Firstly, ACSL4 was overexpressed by transfecting OE-ACSL4 vector in HK-2 cells (Figure 5a,b). Subsequently, the HG-induced increase of MDA and iron and HG-induced decrease of GSH were reversed by SNHG1 knockdown, whereas these effects of SNHG1 knockdown were eliminated following ACSL4 up-regulation (Figure 5c). As shown in Figure 5d, the increased levels of ACSL4, collagen I, collagen IV, and fibronectin, and reduced levels of SLC7A11 and GPX4 induced by HG treatment were antagonized by SNHG1 knockdown, however, the regulatory impacts of SNHG1 knockdown on these proteins

were greatly abolished when ACSL4 was overexpressed. TEM observations indicated that HG-induced mitochondrial contraction, disappearance of the mitochondrial crest, and an increased number of vacuolar mitochondria in HK-2 cells was weakened by SNHG1 knockdown, whereas this effect was reversed by ACSL4 overexpression (Figure 5e). Collectively, SNHG1 knockdown inhibited HG-induced ferroptosis of HK-2 cells via ACSL4.

SNHG1 knockdown inhibited ferroptosis via repressing ACSL4 to alleviate DN in mice

The biological role of SNHG1 regulated ferroptosis in the progression of diabetic nephropathy was further confirmed *in vivo*. SNHG1 was significantly decreased after ferrostatin-1 and shSNHG1 treatments in the kidney tissue of db/db mice (Figure 6a). As shown in Figure 6b, miR-16-5p expression was significantly increased after ferrostatin-1 and shSNHG1 treatments in the kidney tissue of the db/db mice. The ACR, creatinine, and BUN levels were increased in the DN mice, and SNHG1 knockdown or ferrostatin-1 administration markedly down-regulated the above levels (Figure 6c-e). The pathological staining results showed notable morphological changes in the kidneys of db/db mice, including glomerular changes, degeneration of tubular epithelia with loss of brush borders, and tubular lumen dilatation, as well as an obvious expansion of mesangial

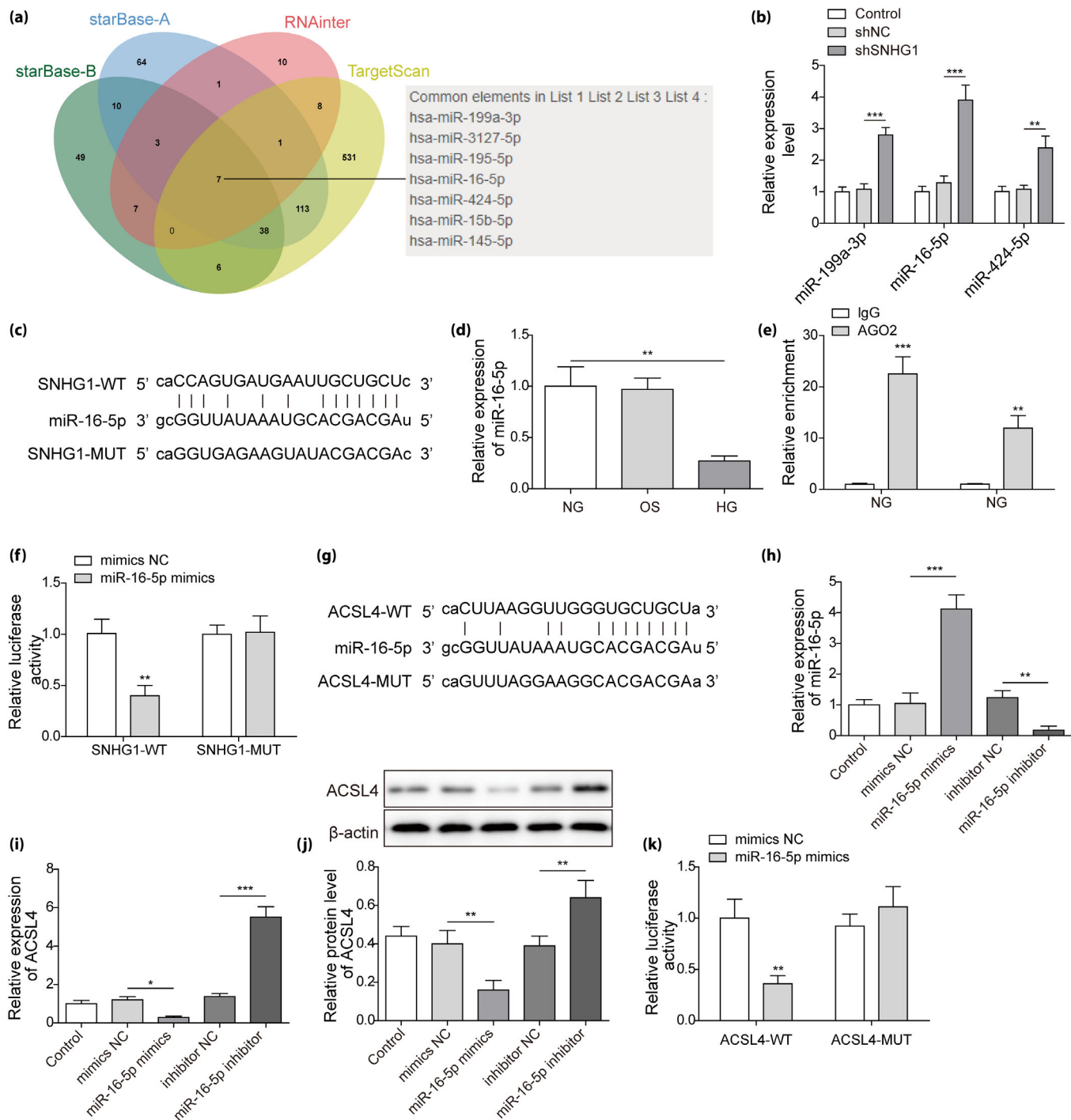


Figure 4 | SNHG1 targeted to miR-16-5p and ACSL4 served as a target for miR-16-5p. (a) the target miRNA downstream of SNHG1 was analyzed by starBase and RNAinter databases, and the target miRNA upstream of ACSL4 was analyzed by starBase and Targetscan databases. (b) miR-199a-3p, miR-16-5p, and miR-424-5p expressions in HK-2 cells after shSNHG1 transfection were detected by qRT-PCR. (c) The binding sequence of SNHG1 and miR-16-5p. (d) qRT-PCR was performed to assess miR-16-5p level in HK-2 cells treated with high glucose. (e,f) The interaction between SNHG1 and miR-16-5p were analyzed using RIP and dual-luciferase reporter gene assays. (g) The downstream target gene of miR-16-5p was predicted by StarBase software. HK-2 cells were transfected with miR-16-5p mimics/inhibitor or mimics/inhibitor NC. (h) qRT-PCR was performed to assess miR-16-5p level. (i,j) qRT-PCR and Western blotting were performed to assess ACSL4 level. (k) Physical interaction between miR-16-5p and ACSL4 was confirmed by dual-luciferase reporter gene assays. ** $P < 0.01$ and *** $P < 0.001$.

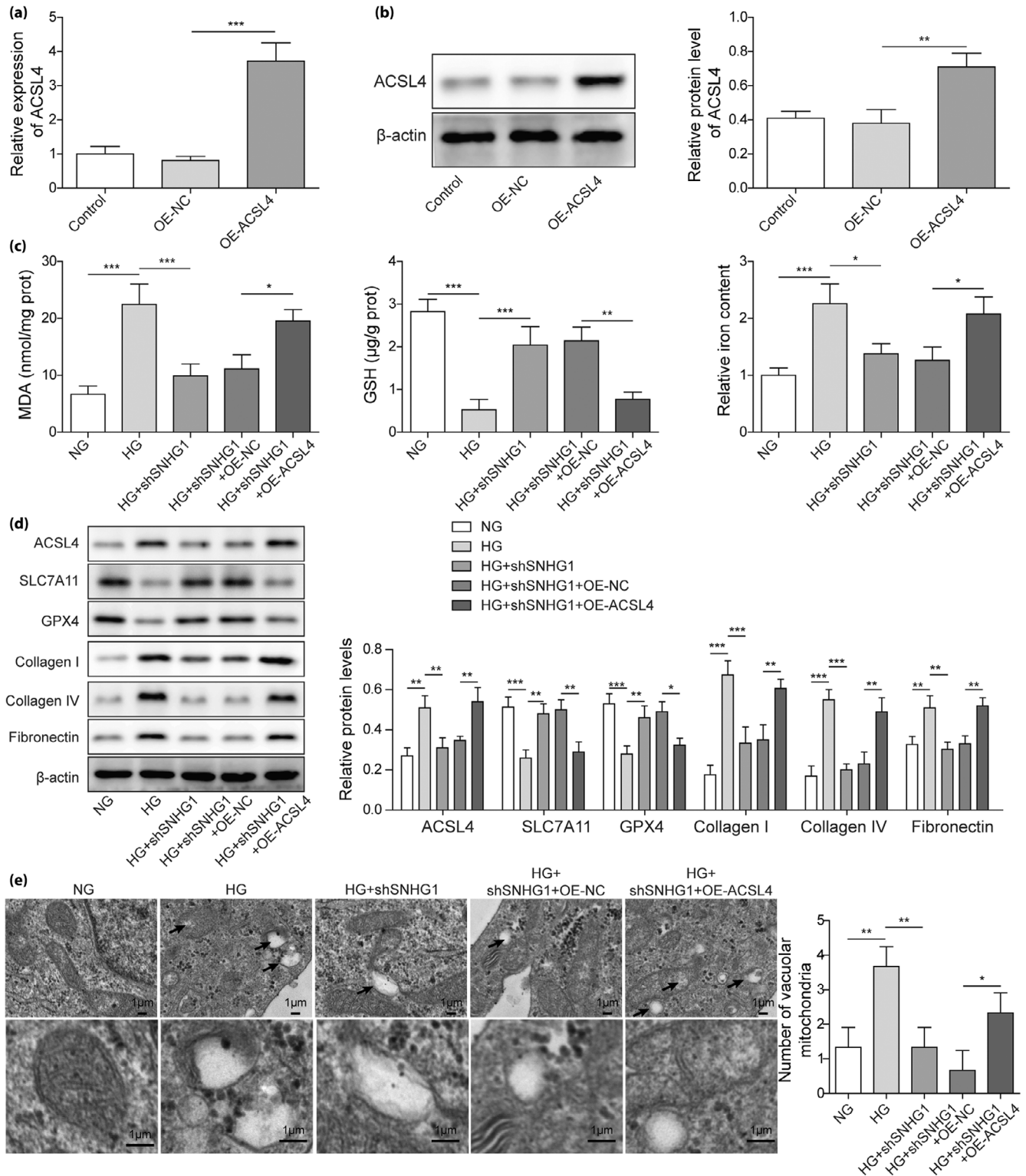


Figure 5 | SNHG1 knockdown inhibited HG-induced ferroptosis of HK-2 cells via ACSL4. HK-2 cells were transfected with OE-ACSL4 or OE-NC. (a,b) qRT-PCR and Western blotting were performed to assess ACSL4 level. HK-2 cells were randomly divided into five groups: NG group, HG group, HG + shSNHG1 group, HG + shSNHG1 + OE-NC group, and HG + shSNHG1 + OE-ACSL4 group. (c) Detection of iron, GSH, and MDA. (d) Western blotting was carried out to assess ACSL4, SLC7A11, GPX4, collagen I, collagen IV, and fibronectin levels. (e) Mitochondrial morphology was observed under TEM, and the number of vacuolar mitochondria was quantitative. **P* < 0.05, ***P* < 0.01 and ****P* < 0.001.

and aggravation of renal fibrosis in the kidneys of db/db mice, while these pathological damages of renal tissue were significantly improved after ferrostatin-1 and shSNHG1 treatment (Figure 6f). As shown in Figure 6g, the NGAL and KIM-1 levels were markedly up-regulated in nephridial tissues, while highly expressed NGAL and KIM-1 were antagonized by SNHG1 knockdown or ferrostatin-1 treatment (Figure 6g). Additionally, MDA and iron levels were enhanced in db/db mice, but GSH expression was reduced, whereas both SNHG1 knockdown or ferrostatin-1 treatment reversed these trends (Figure 6h). The increased ACSL4, collagen I, collagen IV, and fibronectin levels and the reduced SLC7A11 and GPX4 levels were found in db/db mice compared with db/m mice, however, these changes in proteins levels were remarkably antagonized by SNHG1 knockdown or ferrostatin-1 treatment (Figure 6i,j). These findings suggested that SNHG1 knockdown inhibited HG-induced ferroptosis *via* down-regulating ACSL4 *in vivo* (Figure 7).

DISCUSSION

Diabetic nephropathy is traditionally regarded as an inflammatory disease with a highly complex pathogenesis involving a variety of cytokines and molecules²⁹. Some studies have confirmed that oxidative stress induced by HG stimulation might induce the transformation of Fe³⁺ into Fe²⁺ in HK-2 cells, leading to the Fenton reaction and thus inducing cell ferroptosis, and this process might be related to the down-regulation of antioxidant factors³⁰. This paper demonstrated that SNHG1 knockdown inhibited ferroptosis *via* miR-16-5p/ACSL4 axis in diabetic nephropathy, and ferroptosis may be a direction for the treatment of diabetic nephropathy in the future.

Ferroptosis is caused by lipid peroxidation, which is characterized by iron-dependent lipid hydrogen peroxide accumulation to a lethal level³¹. Inhibition of ferroptosis attenuated the development of diabetic nephropathy by up-regulating the Nrf2 level^{31,32}. HMGB knockdown enhanced the proliferation but inhibited ferroptosis in mesangial cells by activating the Nrf2 pathway, thereby alleviating diabetic nephropathy³³. Besides, Prdx6 overexpression prevented multicellular damage by relieving oxidative stress and ferroptosis to inhibit the progression of diabetic nephropathy³⁴. Similarly, our findings indicated that ferroptosis was present in the kidney tissues of db/db mice. Moreover, we also highlighted that HG treatment promoted ferroptosis, and resulted in mitochondrial membrane rupture and mitochondrial cristae disappearance in HK-2 cells, and the above changes could be alleviated by ferrostatin-1 treatment. Overall, these findings confirmed that ferroptosis plays a crucial role in the progression of diabetic nephropathy.

There are growing studies focusing on the role of SNHG1 in diabetes and its complications. As proof, SNHG1 silencing repressed HG-induced ARPE-19 cell inflammation³⁵, but the

roles of SNHG1 in diabetic nephropathy remain unclear. Our results indicate that SNHG1 was highly expressed in diabetic nephropathy, and SNHG1 knockdown inhibited ferroptosis during the progression of diabetic nephropathy. Furthermore, lncRNAs interact with miRNAs through miRNA recognition elements, while miRNA recognition elements serve as “RNA sponges” that can block these molecules, thus reducing their regulation of target mRNAs³⁶. Our study confirmed the interaction between SNHG1 and miR-16-5p. Similar evidence has also been provided by Lei *et al*'s report¹⁰. Importantly, SNHG1 silencing restored miR-16-5p expression in HG-treated HK-2 cells, and miR-16-5p might be an important regulatory target of SNHG1 in the progression of diabetic nephropathy.

It was reported that miR-16-5p reduced LPS-induced lung cancer cell injury by targeting CXCR3³⁷. MiR-16-5p attenuated septicemia induced-acute renal injury by targeting CUL3³⁸. This study indicated the interaction between miR-16-5p and ACSL4. ACSL4 is a sensitive ferroptosis regulator, but it is also an important factor in iron sagging³⁹. ACSL4 mediated the regulation of cardiac remodeling and dysfunctional ferroptosis caused by FUNDC1 deficiency⁴⁰. ACSL4-utilized selenium was required to prevent hydroperoxide-induced ferroptosis⁴¹. Moreover, ACSL4 has been shown to be involved in the regulation of diabetic retinopathy⁴². These findings indicated that ACSL4-mediated ferroptosis may be a potential way to improve diabetes and its complications. Consistently, our findings showed that increased ACSL4 expression enhanced oxidative stress and ferroptosis in HK-2 cells. Moreover, SNHG1 knockdown inhibited HG-induced ferroptosis of HK-2 cells *via* by targeting miR-16-5p to decrease ACSL4, which was confirmed by the *in vivo* mouse DN model.

In summary, our results illustrated that SNHG1 knockdown inhibited HG-induced ferroptosis *via* the miR-16-5p/ACSL4 axis to alleviate diabetic nephropathy in mice. Our study elucidated that diabetic nephropathy was related to ferroptosis, and that ferroptosis may be a direction for the treatment of diabetic nephropathy in the future. Our study provided a new option for the treatment of diabetic nephropathy. Owing to a deeper understanding of disease-relevant miRNAs and mRNAs and advances in *in vivo* delivery systems, the administration of miRNA/mRNA-based therapeutics has recently been shown to be feasible and safe in humans with encouraging efficacy results in early-phase clinical trials⁴³. miR-16-5p implicates an essential role of ferroptosis in diseases^{18,44}. And ACSL4 is a critical determinant of ferroptosis sensitivity which functions in inducing ferroptosis, and its deletion presents an unprecedented resistance to ferroptosis³⁹. Therefore, the administration of miR-16-5p or ACSL4-based therapeutics is a potential treatment strategy for diabetic nephropathy, that is, miR-16-5p activators/ACSL4 inhibitors are potential therapeutic agents for diabetic nephropathy.

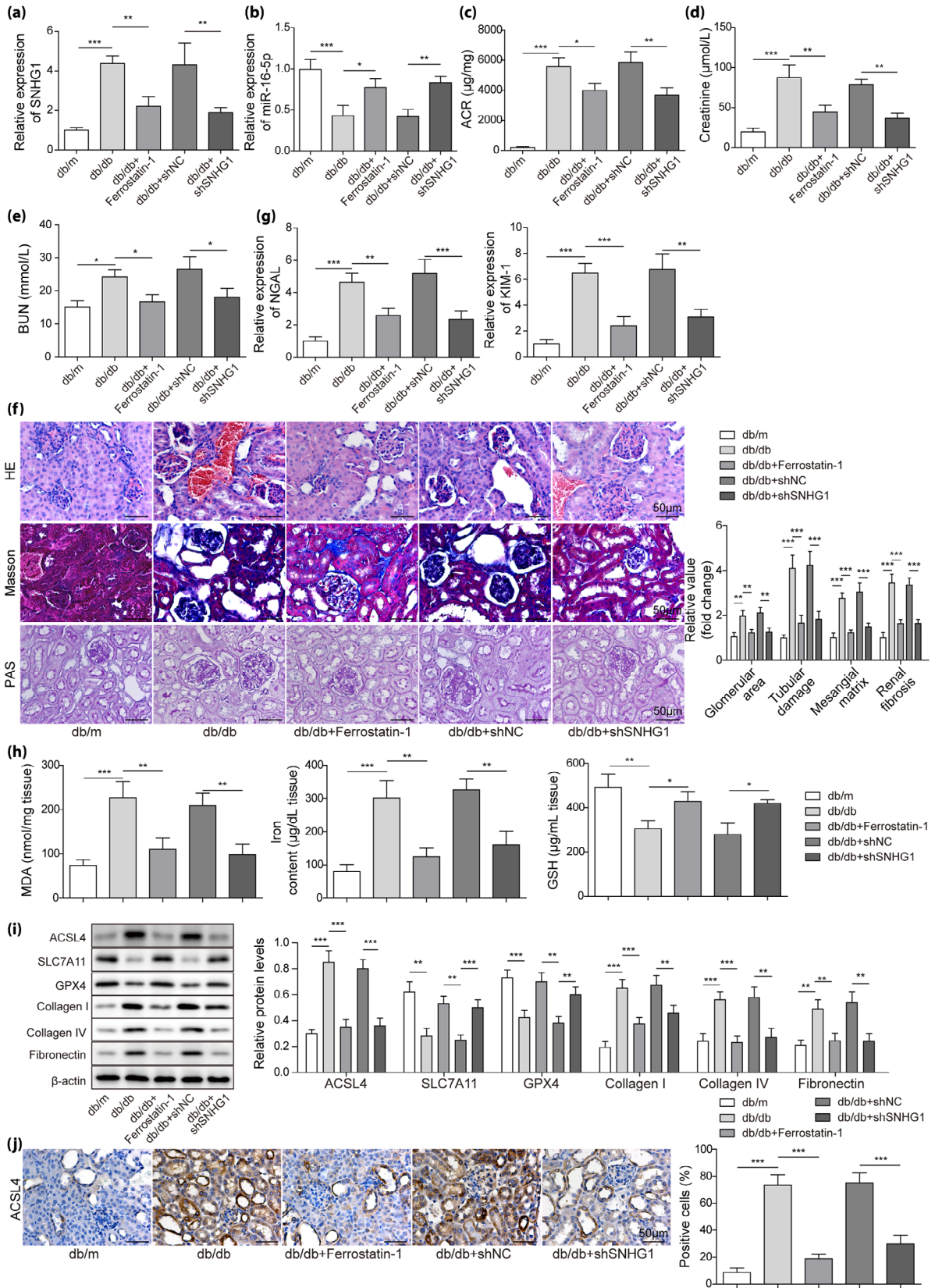


Figure 6 | SNHG1 knockdown inhibited ferroptosis and alleviated diabetic nephropathy in mice. 8-week-old male C57BLKs/J mice were randomly divided into five groups ($n = 8$ per group): db/m group, db/db group, db/db + ferrostatin-1 group, db/db + shNC group, and db/db + shSNHG1 group. (a) SNHG1 expression was detected by qRT-PCR. (b) miR-16-5p expression was detected by qRT-PCR. (c) Ratio of urinary albumin to creatinine (ACR). (d,e) ELISA was performed to detect creatinine and BUN levels. (f) H&E, PAS, and Masson staining were used to assess renal tissue injury, and semi-quantitative analysis of the glomerular area and tubular damage, mesangial scores and the degree of fibrosis are presented. (g) NGAL and KIM-1 expressions were detected by qRT-PCR. (h) Detection of iron, GSH, and MDA. (i) ACSL4, SLC7A11, GPX4, collagen I, collagen IV, and fibronectin levels were assessed by Western blotting. (j) Immunohistochemistry was performed to evaluate the level of ACSL4. * $P < 0.05$, ** $P < 0.01$ and *** $P < 0.001$.

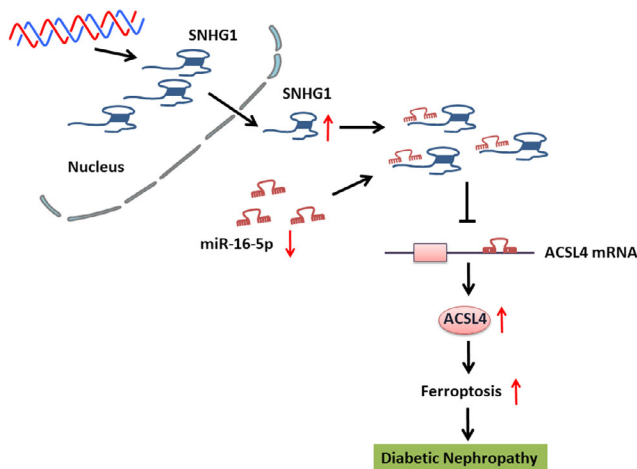


Figure 7 | Schematic diagram.

ACKNOWLEDGMENTS

We would like to give our sincere gratitude to the reviewers for their constructive comments.

DISCLOSURE

There are no conflicts of interest to declare.

Approval of the research protocol: N/A.

Informed consent: N/A.

Approval date of Registry and the Registration No. of the study/trial: N/A.

Animal studies: All animal experiments and protocols were reviewed and approved by the animal care and use Committee of the Second Affiliated Hospital of Nanchang University.

FUNDING

This work was supported by National Natural Science Foundation (82160143) and The Engineering Research Center of Kidney Disease in Jiangxi Province (20164BCD40095).

DATA AVAILABILITY STATEMENT

All data generated or analyzed during this study are included in this published article.

REFERENCES

- Huang H, Zhang G, Ge Z. LncRNA MALAT1 promotes renal fibrosis in diabetic nephropathy by targeting the miR-2355-3p/IL6ST axis. *Front Pharmacol* 2021; 12: 647650.
- A/L B Vasanth Rao VR, Tan SH, Candamy M, et al. Diabetic nephropathy: An update on pathogenesis and drug development. *Diabetes Metab Syndr* 2019; 13: 754–762.
- Terami N, Ogawa D, Tachibana H, et al. Long-term treatment with the sodium glucose cotransporter 2 inhibitor, dapagliflozin, ameliorates glucose homeostasis and diabetic nephropathy in db/db mice. *PLoS One* 2014; 9: e100777.
- Bessho R, Takiyama Y, Takiyama T, et al. Hypoxia-inducible factor-1 α is the therapeutic target of the SGLT2 inhibitor for diabetic nephropathy. *Sci Rep* 2019; 9: 14754.
- Yu MG, Blanquisco L, Arionuevo-Cruz MC. Efficacy of heparinoid supplementation on mortality and disease progression in adults with diabetic kidney disease. *J ASEAN Fed Endocr Soc* 2017; 32: 20–26.
- Hu M, Wang R, Li X, et al. LncRNA MALAT1 is dysregulated in diabetic nephropathy and involved in high glucose-induced podocyte injury via its interplay with β -catenin. *J Cell Mol Med* 2017; 21: 2732–2747.
- Ge X, Xu B, Xu W, et al. Long noncoding RNA GAS5 inhibits cell proliferation and fibrosis in diabetic nephropathy by sponging miR-221 and modulating SIRT1 expression. *Aging (Albany NY)* 2019; 11: 8745–8759.
- Ge Y, Wang J, Wu D, et al. LncRNA NR_038323 suppresses renal fibrosis in diabetic nephropathy by targeting the miR-324-3p/DUSP1 Axis. *Mol Ther Nucleic Acids* 2019; 17: 741–753.
- Lv L, Xi HP, Huang JC, et al. LncRNA SNHG1 alleviated apoptosis and inflammation during ischemic stroke by targeting miR-376a and modulating CBS/H(2)S pathway. *Int J Neurosci* 2021; 131: 1162–1172.
- Lei J, Fu Y, Zhuang Y, et al. LncRNA SNHG1 alleviates IL-1 β -induced osteoarthritis by inhibiting miR-16-5p-mediated p38 MAPK and NF- κ B signaling pathways. *Biosci Rep* 2019; 39: BSR20191523.
- Chen E, Yi J, Jiang J, et al. Identification and validation of a fatty acid metabolism-related lncRNA signature as a predictor for prognosis and immunotherapy in patients with liver cancer. *BMC Cancer* 2022; 22: 1037.
- Yu J, Yu C, Feng B, et al. Intrarenal microRNA signature related to the fibrosis process in chronic kidney disease: Identification and functional validation of key miRNAs. *BMC Nephrol* 2019; 20: 336.

13. Conserva F, Barozzino M, Pesce F, *et al.* Urinary miRNA-27b-3p and miRNA-1228-3p correlate with the progression of kidney fibrosis in diabetic nephropathy. *Sci Rep* 2019; 9: 11357.
14. Zhang A, Li M, Wang B, *et al.* miRNA-23a/27a attenuates muscle atrophy and renal fibrosis through muscle-kidney crosstalk. *J Cachexia Sarcopenia Muscle* 2018; 9: 755–770.
15. Liu L, Wang Y, Yan R, *et al.* BMP-7 inhibits renal fibrosis in diabetic nephropathy via miR-21 downregulation. *Life Sci* 2019; 238: 116957.
16. Assmann TS, Recamonde-Mendoza M, Costa AR, *et al.* Circulating miRNAs in diabetic kidney disease: Case-control study and in silico analyses. *Acta Diabetol* 2019; 56: 55–65.
17. Duan YR, Chen BP, Chen F, *et al.* Exosomal microRNA-16-5p from human urine-derived stem cells ameliorates diabetic nephropathy through protection of podocyte. *J Cell Mol Med* 2021; 25: 10798–10813.
18. Chen Y, Deng Y, Chen L, *et al.* miR-16-5p regulates ferroptosis by targeting SLC7A11 in Adriamycin-induced ferroptosis in cardiomyocytes. *J Inflamm Res* 2023; 16: 1077–1089.
19. Wang Y, Bi R, Quan F, *et al.* Ferroptosis involves in renal tubular cell death in diabetic nephropathy. *Eur J Pharmacol* 2020; 888: 173574.
20. Friedmann Angeli JP, Schneider M, Proneth B, *et al.* Inactivation of the ferroptosis regulator Gpx4 triggers acute renal failure in mice. *Nat Cell Biol* 2014; 16: 1180–1191.
21. Lachiaer E, Louandre C, Godin C, *et al.* Sorafenib induces ferroptosis in human cancer cell lines originating from different solid tumors. *Anticancer Res* 2014; 34: 6417–6422.
22. Tan H, Chen J, Li Y, *et al.* Glabridin, a bioactive component of licorice, ameliorates diabetic nephropathy by regulating ferroptosis and the VEGF/Akt/ERK pathways. *Mol Med* 2022; 28: 58.
23. Kim S, Kang SW, Joo J, *et al.* Characterization of ferroptosis in kidney tubular cell death under diabetic conditions. *Cell Death Dis* 2021; 12: 160.
24. He S, Li R, Peng Y, *et al.* ACSL4 contributes to ferroptosis-mediated rhabdomyolysis in exertional heat stroke. *J Cachexia Sarcopenia Muscle* 2022; 13: 1717–1730.
25. Hong H, Yu H, Yuan J, *et al.* MicroRNA-200b impacts breast cancer cell migration and invasion by regulating ezrin-radixin-Moesin. *Med Sci Monit* 2016; 22: 1946–1952.
26. Jin T, Chen C. Umbelliferone delays the progression of diabetic nephropathy by inhibiting ferroptosis through activation of the Nrf-2/HO-1 pathway. *Food Chem Toxicol* 2022; 163: 112892.
27. Luo M, Gao Z, Li H, *et al.* Selection of reference genes for miRNA qRT-PCR under abiotic stress in grapevine. *Sci Rep* 2018; 8: 4444.
28. Seibert FS, Sitz M, Passfall J, *et al.* Urinary calprotectin, NGAL, and KIM-1 in the differentiation of primarily inflammatory vs. non-inflammatory stable chronic kidney diseases. *Ren Fail* 2021; 43: 417–424.
29. Li A, Peng R, Sun Y, *et al.* LincRNA 1700020114Rik alleviates cell proliferation and fibrosis in diabetic nephropathy via miR-34a-5p/Sirt1/HIF-1 α signaling. *Cell Death Dis* 2018; 9: 461.
30. Wang WJ, Jiang X, Gao CC, *et al.* Salusin- β participates in high glucose-induced HK-2 cell ferroptosis in a Nrf-2-dependent manner. *Mol Med Rep* 2021; 24: 674.
31. Lei P, Bai T, Sun Y. Mechanisms of ferroptosis and relations with regulated cell death: A review. *Front Physiol* 2019; 10: 139.
32. Li S, Zheng L, Zhang J, *et al.* Inhibition of ferroptosis by up-regulating Nrf2 delayed the progression of diabetic nephropathy. *Free Radic Biol Med* 2021; 162: 435–449.
33. Wu Y, Zhao Y, Yang HZ, *et al.* HMGB1 regulates ferroptosis through Nrf2 pathway in mesangial cells in response to high glucose. *Biosci Rep* 2021; 41: BSR20202924.
34. Zhang Q, Hu Y, Hu JE, *et al.* Sp1-mediated upregulation of Prdx6 expression prevents podocyte injury in diabetic nephropathy via mitigation of oxidative stress and ferroptosis. *Life Sci* 2021; 278: 119529.
35. Yang J, Yang K, Meng X, *et al.* Silenced SNHG1 inhibited epithelial-mesenchymal transition and inflammatory response of ARPE-19 cells induced by high glucose. *J Inflamm Res* 2021; 14: 1563–1573.
36. Huang Y. The novel regulatory role of lncRNA-miRNA-mRNA axis in cardiovascular diseases. *J Cell Mol Med* 2018; 22: 5768–5775.
37. Liu GP, Wang WW, Lu WY, *et al.* The mechanism of miR-16-5p protection on LPS-induced A549 cell injury by targeting CXCR3. *Artif Cells Nanomed Biotechnol* 2019; 47: 1200–1206.
38. Xu G, Mo L, Wu C, *et al.* The miR-15a-5p-XIST-CUL3 regulatory axis is important for sepsis-induced acute kidney injury. *Ren Fail* 2019; 41: 955–966.
39. Doll S, Proneth B, Tyurina YY, *et al.* ACSL4 dictates ferroptosis sensitivity by shaping cellular lipid composition. *Nat Chem Biol* 2017; 13: 91–98.
40. Pei Z, Liu Y, Liu S, *et al.* FUNDC1 insufficiency sensitizes high fat diet intake-induced cardiac remodeling and contractile anomaly through ACSL4-mediated ferroptosis. *Metabolism* 2021; 122: 154840.
41. Ingold I, Berndt C, Schmitt S, *et al.* Selenium utilization by GPX4 is required to prevent hydroperoxide-induced ferroptosis. *Cell* 2018; 172: 409–422.e21.
42. Liu C, Sun W, Zhu T, *et al.* Glia maturation factor- β induces ferroptosis by impairing chaperone-mediated autophagic degradation of ACSL4 in early diabetic retinopathy. *Redox Biol* 2022; 52: 102292.
43. Su Q, Lv X. Revealing new landscape of cardiovascular disease through circular RNA-miRNA-mRNA axis. *Genomics* 2020; 112: 1680–1685.
44. Li J, Yan X, Li B, *et al.* Identification and validation of ferroptosis-related genes in patients infected with dengue virus: Implication in the pathogenesis of DENV. *Virus Genes* 2023; 59: 1–14.

SUPPORTING INFORMATION

Additional supporting information may be found online in the Supporting Information section at the end of the article.

Figure S1 | SNHG1 knockdown inhibited HG-induced ferroptosis of mouse mesangial cells and mouse podocytes. Mouse mesangial cells (SV40-MES13) and mouse podocytes (MPC5) were transfected with shSNHG1 or shNC. (a) qRT-PCR was performed to assess the SNHG1 level. SV40-MES13 and MPC5 cells were divided into six groups: NG group, HG group, erastin group (positive control), HG + shNC group, HG + shSNHG1 group, and HG + ferrostatin-1 group. (b) Detection of iron, GSH, and MDA. (c) ACSL4, SLC7A11, and GPX4 levels were measured by Western blotting. * $P < 0.05$, ** $P < 0.01$ and *** $P < 0.001$.